2.C

Nuclear Physics A263 (1976) 61—74; © *North-Holland Publishing Co., Amsterdam*

17

SYSTEMATICS OF THE VALENCE CAPTURE MODEL FOR LOW-ENERGY NEUTRON RADIATIVE CAPTURE

J. CUGNON

University of Liège, Institute of Physics, Sart Tilman, B-4000 Liège I (Belgium)

Received 29 December 1975

Abstract: The factor of proportionality between the partial photon width and the elastic channel neutron width, introduced by the valence model, is calculated for a large fraction of the periodic table. Results are presented in such a way that they can be used very easily for the analysis of experimental data. Background capture cross sections are estimated for the 4s region. The importance of the inelastic channel components, which are neglected in the valence model, is studied. Their contribution is estimated numerically in some cases.

1. Introduction

The valence capture model has proved useful in the analysis of low-energy neutron radiative capture. In particular, it can explain the observed correlation between radiative partial width for electric dipole radiation and the neutron width, and it also accounts for the existence of the correlation between the photon intensities for electric dipole transitions leading to different final states and the neutron spectroscopic factors of these final states. Essentially, the model assumes that the components which contribute to the process are, in the initial (scattering) and final states, those which describe the target in its ground state; the "inert core components". It has been stressed in recent papers [1,2]) that if only these components are involved, the radiative process mainly takes place outside the nucleus, two or three fm beyond the nuclear radius. The inert core component in the initial (resonant) state is then proportional to the reduced neutron width. Hence, the radiative partial width is also proportional to the same quantity. Lane and Lynn [3,4]) derived, a long time ago, an expression for this factor of proportionality. However, their result strictly holds at zero neutron energy. Recently, Lane and Mughabghab [5]) derived a fairly general expression for the proportionality factor, which is valid for non-zero neutron energy. They also gave an expression for the radiative capture background cross section. The formulae involve optical-model quantities.

The whole problem has also been reinvestigated [2]) in the frame of the shell-model [6]) or Feshbach reaction theory [7]). The work of ref. [2]) contains three important conclusions: (i) the factor of proportionality can be equivalently given in terms of complex or real optical-model potential; (ii) what is usually measured experimentally is not the parameters of the S- (or K-) matrix, but slightly different quantities; (iii)

the potential used for calculating the background cross section may be real or complex, but it has to reproduce the optical nucleon-nucleus scattering length.

The validity of the valence model lies in the small size of the contribution of the excited target components to the radiative width. This question has been investigated in refs. [2, 8]). In ref. [8]), Lane discussed qualitatively the neutron reduced width for excited target state (or closed) channels, while ref. [2]) mainly deals with the energy dependence of the factor of proportionality when the neutron energy is negative. We reinvestigate globally the problem here.

In fact, the aim of this paper is fourfold: (i) We want to do a systematic study of the valence model for the 2p, 3s, 3p and 4s regions. (ii) We calculate, within the valence model, the factor of proportionality between the elastic channel contribution to the radiative partial width and the neutron width in this channel. We try to present the results in such a way that they can be used easily by experimentalists. (iii) We estimate the value of the background cross section in the 4s region. (iv) We discuss the question of the inelastic channel contribution to the photon width and try to evaluate it in some cases.

In sect. 2, we recall the main features of the valence model. Sect. 3 is devoted to the numerical calculation of the factor of proportionality mentioned above in different regions of the periodic table. In sect. 4, we briefly discuss the value of the background cross section at low energy. In sect. 5 we turn to the inelastic channel contribution. Finally, sect. 6 contains our conclusions.

2. The valence capture model

We assume that the elastic neutron channel (n) is the only open particle channel. The collision matrix can be written as

$$S_{nn} = e^{2i\delta_0}\frac{1+i\tilde{K}_{nn}}{1-i\tilde{K}_{nn}}, \qquad S_{nf} = -2ie^{i\delta_0}\frac{\tilde{K}_{nf}}{1-i\tilde{K}_{nn}}, \tag{2.1}$$

where f refers to a given photon channel and where

$$\tilde{K}_{nn} = \tilde{K}^0_{nn} + \tfrac{1}{2}\sum_\lambda \frac{\tilde{\Gamma}_{\lambda n}}{\tilde{E}_\lambda - E}, \qquad \tilde{K}_{nf} = \tilde{K}^0_{nf} + \tfrac{1}{2}\sum_\lambda \frac{\tilde{\Gamma}^{\frac{1}{2}}_{\lambda f}\tilde{\Gamma}^{\frac{1}{2}}_{\lambda n}}{E_\lambda - E}. \tag{2.2}$$

It is argued in ref. [2]) that the quantities $\tilde{\Gamma}_{\lambda f}$ and $\tilde{\Gamma}_{\lambda n}$ can be identified with the measured photon and neutron width if δ_0 is the background neutron elastic phase shift. The latter can be taken as the real part of the optical phase shift. In the context of the valence model, one has [2])

$$\tilde{\Gamma}^{\frac{1}{2}}_{\lambda f} = -\tilde{\Gamma}^{\frac{1}{2}}_{\lambda n}\theta_f \frac{\mathrm{Im}\,\{\langle t_f|d|u_{opt}\rangle \cos\delta_{opt}/\cos(\delta_{opt}-\delta_0)\}}{\mathrm{Im}\tan(\delta_{opt}-\delta_0)}, \tag{2.3}$$

where u_{opt} is the optical wave function and where d is the electric dipole operator relative to the incident neutron and suitably normalized. The quantities θ_f and t_f are the neutron spectroscopic factor of the final state and the corresponding single-particle wave function, respectively. Eq. (2.3) generalizes the Lane-Mughabghab expression, which can be recovered by putting $\delta_0 = 0$. In practice, the difference is rather small, since δ_0 is small †.

The valence capture model also predicts the magnitude of the background cross section for radiative capture. The expression of the background S-matrix element is

$$S^{BG}_{nf} = -2i\frac{\mathrm{Re}\,\{\langle t_f|d|u_{opt}\rangle \cos\delta_{opt}(\cos(\delta_{opt}-\delta_0))^{-1}\}}{1-i\,\mathrm{Re}\tan(\delta_{opt}-\delta_0)}. \tag{2.4}$$

In ref. [2]), it is shown that expression (2.4) is quite sensitive to the optical-model potential. Arguments are given which say that expression (2.4) can only be interpreted as the physical background cross section if the optical-model potential reproduces the optical scattering length correctly. We also require this property for the optical potential that is introduced in eq. (2.3), although the r.h.s. of eq. (2.3) is fairly independent of the phenomenological optical potentials which are available.

3. Systematics of the elastic channel contribution

Let us consider a specific case with an initial scattering state Ψ^J_E and a given final state $\Psi^{J'}_f$. We have, neglecting antisymmetrization

$$\Psi^J_E = \sum_i \sum_s \{u_i(E^s_n)\Phi_s\}_J, \tag{3.1a}$$

$$\Psi^{J'}_f = \sum_j \sum_t \theta_{t,j}\{t_j\Phi_t\}_{J'}, \tag{3.1b}$$

where the Φ are the target states. The functions $u_i(E^s_n)$ describe the motion of the neutron with a set of quantum numbers denoted by i and with an energy $E^s_n = E - E_s$. The functions t_j are neutron bound state wave functions normalized to unity. Finally, the square of $\theta_{t,j}$ is the corresponding spectroscopic factor. Essentially, the valence model assumes that the components along the target ground state Φ_0 are the only important ones both in Ψ^J_E and in $\Psi^{J'}_f$. The initial and final single-particle states generally satisfy the selection rules for electromagnetic radiation. For E1 transition, as considered here, the main transitions are 2p → 2s, 3s → 2p, 3p → 3s and 4s → 3p. The spin algebra is different if the spin-orbit splitting is taken into account. Moreover, the formulae are more complicated for non-zero targets. The general formulae for the geometrical factor can be found in ref. [9]). We give below explicit formulae for the different cases.

3.1. THE s → p TRANSITIONS

For a zero-spin target, the spin of the resonances is $\frac{1}{2}$. Let us first assume that we

† Actually, the Lane-Mughabghab result applies to average partial widths. But another expression which refers to individual resonance parameters has been worked out in ref. [2]) and has been shown to be equivalent to the optical-model expression.

know the total angular momentum j_f of the neutron in the final state. In this case, we have

$$\frac{\tilde{\Gamma}_{\lambda f}}{\tilde{\Gamma}_{\lambda n}} = \delta\theta^2_{j_f}\varepsilon_\gamma^3\frac{Z^2}{A^2}\mathscr{A}(j_f)k_n^{-1}|\mathscr{J}(j_i, j_f)|^2, \tag{3.2}$$

where

$$\delta = \frac{8\pi^2}{9}\frac{e^2}{(\hbar c)^3} = 1.64412\times10^{-6}\ \mathrm{MeV}^{-2}\cdot\mathrm{fm}^{-2}, \tag{3.3}$$

and where k_n is the incident neutron wave number. The quantity ε_γ is the photon energy; Z and A are the charge and mass numbers of the residual nucleus; and $\mathscr{A}$ is a geometrical factor whose value is given by

$$\mathscr{A}(j_f = \tfrac{3}{2}) = \frac{1}{2\pi}, \qquad \mathscr{A}(j_f = \tfrac{1}{2}) = \frac{1}{4\pi}. \tag{3.4}$$

The explicit expression for $\mathscr{J}(j_i, j_f)$ is

$$\mathscr{J}(j_i, j_f) = \frac{\mathrm{Im}\,\{\langle t_{j_f}|r|u_{\mathrm{opt},j_i}\rangle\cos\delta_{\mathrm{opt}}[\cos(\delta_{\mathrm{opt}}-\delta_0)]^{-1}\}}{\mathrm{Im}\tan(\delta_{\mathrm{opt}}-\delta_0)}, \tag{3.5}$$

where the optical wave function behaves asymptotically like

$$u_{\mathrm{opt},j_i} \sim r^{-1}\sqrt{\frac{2M}{\pi\hbar^2}}(\sin k_n r + \tan\delta_{\mathrm{op}}\cos k_n r), \tag{3.6}$$

for $l = 0$. In the following we take $\delta_0 = \mathrm{Re}\,\delta_{\mathrm{opt}}$, as in ref. [2]).

If the target spin is non-zero, the spin algebra is a little more complicated. The neutron can be transferred in $p_{\frac{3}{2}}$ and $p_{\frac{1}{2}}$ orbits in the same final state. Moreover, the $\mathscr{A}$-factor now depends on the spin of the target I_A, the spin of the resonance J and the spin of the residual nucleus I_B. We have

$$\frac{\tilde{\Gamma}_{\lambda f}}{\tilde{\Gamma}_{\lambda n}} = \delta\varepsilon_\gamma^3\frac{Z^2}{A^2}\Big|\sum_{j_f=\frac{3}{2},\frac{1}{2}}\theta_{j_f}\mathscr{A}^{\frac{1}{2}}(I_A, J, I_B, j_f)\mathscr{J}(j_i = \tfrac{1}{2}, j_f)\Big|^2 k_n^{-1}. \tag{3.7}$$

Experimentally, at best the quantities $|\theta_{j_f}|^2, j_f = \frac{3}{2}$ or $\frac{1}{2}$, are known and not the relative phases. Moreover, in practice, only the spectroscopic factor $\bar{\theta}^2$ for the capture in the p-state is known, irrespective of the j-value. The quantity $\bar{\theta}^2$ is a weighted sum of the $\theta^2_{j_f}$. Eq. (3.7) can be conveniently simplified by neglecting the cross terms and by assuming that the weight is given by the $\mathscr{A}$-factors. We then obtain

$$\frac{\tilde{\Gamma}_{\lambda f}}{\tilde{\Gamma}_{\lambda n}} = \delta\varepsilon_\gamma^3\frac{Z^2}{A^2}\bar{\theta}^2\frac{1}{4\pi}\frac{2I_B+1}{2J+1}k_n^{-1}\overline{|\mathscr{J}(j_i = \tfrac{1}{2}, j_f)|^2}^{\,j_f}. \tag{3.8}$$

The bar means the arithmetic average over the index j_f.

3.2. THE p → s TRANSITIONS

For zero spin targets, we have

$$\frac{\tilde{\Gamma}_{\lambda f}}{\tilde{\Gamma}_{\lambda n}} = \delta\theta^2_{j_f}\varepsilon_\gamma^3\frac{Z^2}{A^2}\mathscr{A}(j_i)k_n^{-3}|\mathscr{J}(j_i, j_f)|^2, \tag{3.9}$$

where

$$\mathscr{A}(j_i = \tfrac{3}{2} = J) = \frac{1}{4\pi} = \mathscr{A}(j_i = \tfrac{1}{2} = J). \tag{3.10}$$

The quantity $\mathscr{J}$ is given by eq. (3.5) where the normalization of the optical wave function is determined by the asymptotic form ($l = 1$)

$$u_{\mathrm{opt},j_i} \sim \frac{1}{r}\sqrt{\frac{2Mk_n^2}{\pi\hbar^2}}(\cos k_n r - \tan\delta_{\mathrm{opt}}\sin k_n r). \tag{3.11}$$

For a non-zero spin target, and if the resonant state of spin J can be populated by $p_{\frac{3}{2}}$ as well as $p_{\frac{1}{2}}$, the neutron width is generally not known for each channel, but only for the $l = 1$ channel considered as a whole. In that case, one can use the formula

$$\frac{\tilde{\Gamma}_{\lambda f}}{\tilde{\Gamma}_{\lambda n}} = \delta\theta^2_{j_f}\varepsilon_\gamma^2\frac{Z^2}{A^2}k_n^{-3}\sum_{j_i=\frac{1}{2},\frac{3}{2}}\frac{\langle j_i m_i I_A I_A|JJ\rangle^2}{2J+1}\frac{1}{4\pi}|\mathscr{J}(j_i, j_f)|^2. \tag{3.12}$$

3.3. USE OF THE GRAPHS

We give in the figures below the value of the quantities $|\mathscr{J}(j_i, j_f)|$ for different regions. For p → s transitions, the curves are given up to 500 keV neutron energy. For s → p transitions, the curves are given to 200 keV, but we checked that they can be extended linearly up to 500 keV, with an error less than a few percent. The quantities $|\mathscr{J}(j_i, j_f)|$ are given for several values of A. For the other values of A, one can use linear interpolation.

3.4. DISCUSSION

3.4.1. The 3s region. The optical potential which best reproduces the scattering length in this region is the Moldauer potential [10]), and this is the one we have taken. As in subsect. 3.4, the final single-particle wave function is calculated from the potential given by Ross *et al.* [11]), which provides good single-particle wave functions near the Fermi level for a wide range of nuclei: the real part of Moldauer potential overbinds the 2p levels by 3 or 4 MeV. Let us note, however, that the results are not very sensitive to the very detail of the function t_f. The results of the calculation of $\mathscr{J}$ are given in fig. 1. Except for very small energies, the quantities $|\mathscr{J}|$ are linear functions of the neutron energy. The general trend is a decrease of $|\mathscr{J}|$ with the mass number. This is due, as explained in ref. [2]), to the fact that the wave function t_{j_f} (eq. (3.5)) is pushed more and more inside the nucleus and that external capture

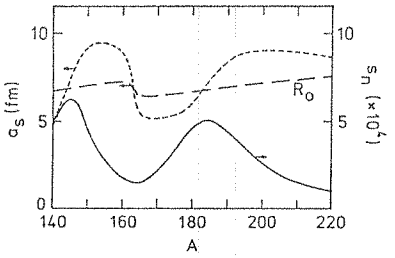

Fig. 1. Calculation of the quantity $|\mathscr{J}|$ (see the text) versus the neutron energy E_n in the 3s region. The numbers labelling the curves are the mass numbers.

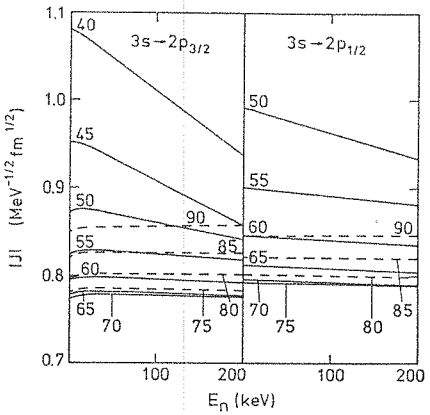

Fig. 2. Neutron strength function (full curve, normalized at 1 eV), scattering length a_s (small dashes) and radius (long dashes) corresponding to the optical-model potential used in the 4s region (see the text for detail).

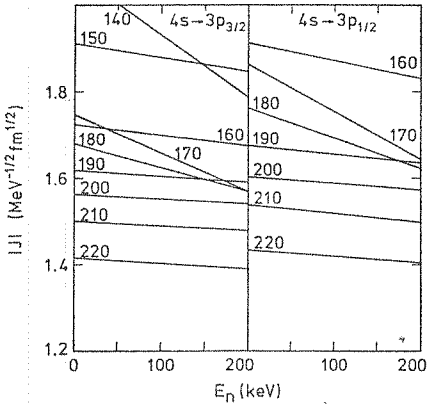

Fig. 3. Same as fig. 1 for the 4s region.

dominates. The difference between the $3s_{\frac{1}{2}} \rightarrow 2p_{\frac{3}{2}}$ and $3s_{\frac{1}{2}} \rightarrow 2p_{\frac{1}{2}}$ transitions has essentially the same origin.

3.4.2. The 4s region. In this region, the measurements of the scattering length are very scarce. We are thus reduced to choosing the optical potential which best reproduces the strength function, hoping that the scattering length and the strength function are reproduced with the same accuracy, which seems to be the case in the 3s region. The best optical potential in the 4s region must contain vibrational and rotational couplings in order to account for the splitting of the 4s giant resonance. Since a good description of the s-wave part of the optical wave function is only

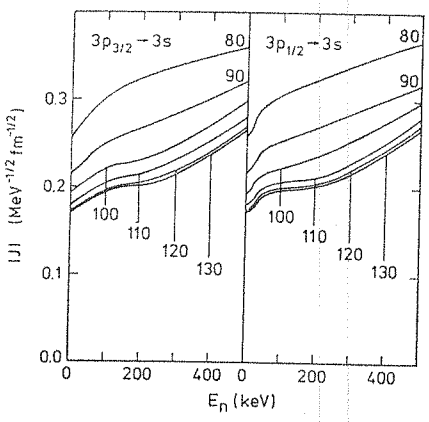

Fig. 4. Same as fig. 1 for the 3p region.

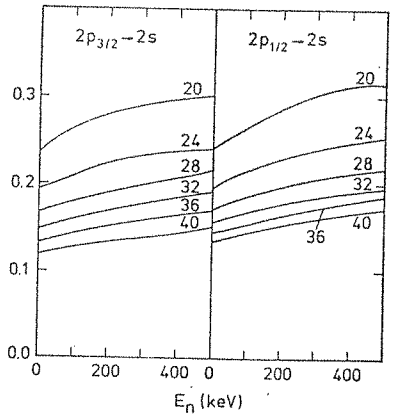

Fig. 5. Same as fig. 1 for the 2p region.

needed outside the nucleus, we avoid the complications of these couplings and use a spherically symmetric optical potential. We vary the radius parameter in such a way that the strength function is reproduced (on the average). The other parameters are those of the spherical part of Jain's optical potential [12]). The results of the fit for the strength function are given in fig. 2, as well as the value of the corresponding scattering length.

The values of the calculated $|\mathscr{J}|$ quantities are given in fig. 3. Once again, they are linear in the energy. The general trend of the A-dependence is the same as in the 3s region, with, however, some slight differences induced by the splitting of the giant resonance. The average value of $|\mathscr{J}|$ is larger in the 4s region than in the 3s region. This is easily interpreted as the effect of the r-operator in eq. (3.7) conjugated with the dominance of external capture.

3.4.3. The 3p region. Once again, because of the lack of scattering length measurements, we are reduced to choose the optical potential that provides the best fit to the p-strength function. Moldauer's potential is the most suitable one, at least at the centre of the giant resonance. The values of $|\mathscr{J}|$ are given in fig. 4. The curves seem more complicated than those relative to the 3s and 4s cases. However, the gross variation with A is the same. The (slight) difference between the $p_{\frac{3}{2}}$ and the $p_{\frac{1}{2}}$ captures arises from the fact that the $p_{\frac{3}{2}}$ wave experiences a less repulsive potential than the $p_{\frac{1}{2}}$ wave at the exterior of the nucleus, where most of the capture takes place.

3.4.4. The 2p region. In this region, the best optical potential is quite badly determined. We have taken the same optical model as in the 3p region. The results are shown in fig. 5.

3.5. REMARK CONCERNING THE DIPOLE OPERATOR

In subsects. 3.1 and 3.2, we have assumed that the electric dipole operator d is essentially given by

$$d = \varepsilon_{if} r \cdot \varepsilon, \tag{3.13}$$

where ε_{if} is the energy of the transition, and where ε is polarization vector of the photon. The operator d can also be defined with the help of the gradient operator. When d is sandwiched between two states which are not orthogonal [as in eq. (3.5)], an ambiguousity arises, since the relation

$$-\frac{m}{\hbar^2}\varepsilon_{if}\langle \mathrm{i}|r\cdot\varepsilon|\mathrm{f}\rangle = \langle \mathrm{i}|\nabla\cdot\varepsilon|\mathrm{f}\rangle \tag{3.14}$$

is no longer valid. The numerical results described below are obtained with the form (3.13). We checked that using the gradient form does not change very much the values of $\Gamma_{\lambda f}/\Gamma_{\lambda n}$, say less than ten percent, except in the wings of the giant resonances, where the difference can reach 20 %. The background cross section may change more than 50 %. We, however, preferred to use (3.13), since the gradient form corresponds to a current which is not conserved, while Siegert's theorem [15]) tells us that the current $[H, r]$, which yields eq. (3.13), is conserved.

4. The background cross section

Besides the correlation between photon and neutron widths, the valence capture model predicts the existence of a background capture. This provides a challenge to experimentalists. However, up to now, the existence of a background cross section has not been established unambiguously. The predictions, within the valence capture model, of the most favourable regions of the periodic table for the observation of sizeable background capture cross sections would be desirable. In the following, we restrict ourselves to s-wave capture, since the background p-wave capture cross section would be too small. The background cross section is given for a s $\rightarrow (l = 1, j_f)$ capture on a zero-spin target by

$$\sigma_{n\gamma}^{BG} = \frac{\pi\delta}{k_n^2}\theta_{j_f}^2\varepsilon_\gamma^3\frac{Z^2}{A^2}\mathscr{A}(j_f)|I(j_i, j_f)|^2, \tag{4.1}$$

where $\mathscr{A}$ is given by eq. (3.4) and where

$$|I(j_i, j_f)| = 2\left|\frac{\mathrm{Re}\,\{\langle t_{j_f}|r|u_{\mathrm{opt},j}\rangle\cos\delta_{\mathrm{opt}}[\cos(\delta_{\mathrm{opt}}-\delta_0)]^{-1}\}}{1 - i\,\mathrm{Re}\tan(\delta_{\mathrm{opt}}-\delta_0)}\right|. \tag{4.2}$$

If the average over j_f is taken, or if the spin of the target in non-zero, eq. (4.1) should be changed in the way described in sect. 3.

The calculation for the background has been performed in ref. [2]) for the 3s region. According to these results, the background is more likely to be observed for $A \lessapprox 55$.

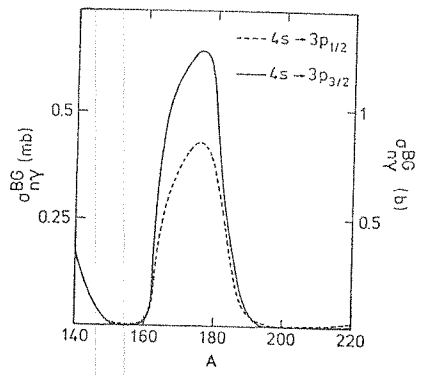

Fig. 6. Calculated background cross section in the 4s region. The curves give, within 1 or 2 %, the cross sections both 100 keV neutrons (left-hand scale) and for thermal neutrons (right-hand) scale.

We give in fig. 6 the results for the 4s region, using the same optical potential as in subsect. 3.4.2. We have put $\theta_{j_f}^2 = 1$. We see that the most favourable region for the observation of the background extends from $A \approx 170$ to $A \approx 190$. At low energy the cross section is inversely proportional to k_n because of threshold effect. This effect extends to $E_n \approx 100$ keV, and factors out from the remaining expression which contains all the A-dependence. The curve in fig. 6 represents the background cross section for $0 < E_n \lessapprox 100$ keV, provided that the quantities $\sigma_{n\gamma}^{BG}(E_n)$ are given by

$$\sigma_{n\gamma}^{BG}(E_n) = \sigma_{n\gamma}^{BG}(100\ \mathrm{keV})\sqrt{(100\ \mathrm{keV})/E_n}.$$

5. The closed channel contribution

To be specific, let us consider the 3s region. The underlying single-particle transition is 3s → 2p. We kept only these components in Ψ_E^J and $\Psi_f^{J'}$ (eq. (3.1)), with the target in its ground state. If the energy is sufficiently low, say less than 100 or 200 keV, there is no open inelastic neutron channel in general. Then, the other components in (3.1a) correspond to a negative neutron energy, i.e. a closed channel. This fact explains the title of this section.

Let us call d the dipole operator relative to the neutron and D the dipole operator corresponding to the target. The E1$(= d+D)$ matrix element should read, using eqs. (3.1), and neglecting antisymmetrization between the incident neutron and the nucleons of the core,

$$\begin{aligned}\langle\Psi_E^J|\mathrm{E1}|\Psi_f^{J'}\rangle &= \theta_{0,2p}\langle\{u_{3s}(E_n^0)\Phi_0\}_J|d|\{t_{2p}\Phi_0\}_{J'}\rangle \\ &+ \sum_i\sum_{[j]}\sum_{s\neq 0}\theta_{s,j}\langle\{u_i(E_n^i)\Phi_s\}_J|d|\{t_j\Phi_s\}_{J'}\rangle \\ &+ \sum_i\sum_{[s]}\sum_{s'\neq 0}\theta_{s',i}\langle\{u_i(E_n^i)\Phi_s\}_{J'}|D|\{t_i\Phi_{s'}\}_{J'}\rangle.\end{aligned} \tag{5.1}$$

The first term is the one retained in the valence model picture. In the second term, the symbol $[j]$ means that one only retained the t_j which have non-vanishing matrix elements with the u_i. The symbol $[s]$ in the third term has a similar meaning. An interesting part of this term is provided by the case where $s' = 0$ and s denotes the giant dipole state constructed on Φ_0. We do not examine these transitions here. We refer to recent works [1, 2]) where they are discussed and where it is argued that they are not important near the neutron emission threshold.

Let us discuss in more detail the second term in (5.1). In general †, only one single-particle giant resonance among all the partial waves involved is important. In other words, the wave functions u_i corresponding to a given partial wave dominates the other ones. Around $A = 60$, it is the 3s partial wave. Hence, in the second term, the summation over i can be reduced to one term. The summation over j is also reduced because of the selection rule. Neglecting the third term in (5.1), we have

$$\langle \Psi_E^J | \mathrm{E1} | \Psi_f^{J'} \rangle = \theta_{0,2p} \langle \{u_{3s}(E_n^0)\Phi_0\}_J | d | \{t_{2p}\Phi_0\}_{J'} \rangle + \theta_{1,2p} \langle \{u_{3s}(E_n^1)\Phi_1\}_J | d | \{t_{2p}\Phi_1\}_{J'} \rangle + \theta_{2,2p} \ldots . \quad (5.2)$$

This decomposition also applies to partial photon width, and we write with obvious notation

$$\Gamma_{\lambda f}^{\downarrow} = \Gamma_{\lambda f,0}^{\downarrow} + \Gamma_{\lambda f,1}^{\downarrow} + \Gamma_{\lambda f,2}^{\downarrow} + \ldots . \quad (5.3)$$

We have neglected the (small) difference between the quantities with and without tildes [$\delta_0 = 0$ in eqs. (2.1) and (2.2)]. In eq. (5.2) E_n^1 is negative, in general, at low energy. The quantity $\Gamma_{\lambda f,0}^{\downarrow}$ is of course given by eq. (2.3) (with $\delta_0 = 0$). A straightforward generalization of the latter equation to negative neutron energy yields an expression for

$$\Gamma_{\lambda f,1}^{\downarrow} = \Gamma_{\lambda n,1}^{\downarrow} \theta_{1,2p} \frac{\mathrm{Im}\,\{\langle t_{2p}|d|u_{opt}(E_n^1)\rangle/(\cos\delta_{opt} + \sin\delta_{opt})\}}{\mathrm{Im}\,(S_{opt})}, \quad (5.4)$$

where the optical model quantities refer now to the channel $\{u_{3s}\Phi_1\}_J$ with a negative energy E_n^1. The optical wave is represented by ($l = 0$)

$$u_{opt} \approx \frac{1}{r}\sqrt{\frac{2M}{\pi\hbar^2\kappa}}\,(S(r)\cos\delta_{opt} + C(r)\sin\delta_{opt}), \quad (5.5)$$

with for s-wave,

$$S(r) \approx \mathrm{sh}\,\kappa r, \qquad C(r) \approx \mathrm{ch}\,\kappa r, \qquad -\hbar^2\kappa^2/2m = E_n^1. \quad (5.6)$$

Evidently, one has

$$S_{opt} = \frac{1 - \tan\delta_{opt}}{1 + \tan\delta_{opt}}. \quad (5.7)$$

† An exception is, for instance, given by the interference of the 4s and 3d giant resonances around $A \approx 160$.

The S-matrix enters explicitly in eq. (5.4) since, at negative energies, the physical poles and residues are those of the S-matrix. We draw the attention to the quantity $\Gamma_{\lambda n,1}$, which is defined as the residue of the pole of the S-matrix in the channel $\{u_{3s}\Phi_1\}_J$. This pole manifests itself as a resonance in channel 0, but is located below the inelastic threshold. Hence, $\Gamma_{\lambda n,1}$ is not directly accessible by experiment.

We can summarize eqs. (5.2) and (2.3) by writing

$$\Gamma_{\lambda f,i} = (\theta_{i,2p})^2 \zeta(i) \Gamma_\lambda(E_n^i) f(E_n^i), \qquad i = 0, 1, 2, \ldots, \quad (5.8)$$

where

$$\zeta(i) = \delta\varepsilon_\gamma^3 \mathscr{A}(i). \quad (5.9)$$

The function $f(E_n^i)$ is given by

$$f(E_n^i) = k_n^{-1} \mathscr{J}(j_i, j_f)|^2, \quad (5.10a)$$

if $i = 0$ [see eq. (3.7)] and by

$$f(E_n^i) = \left| \frac{\mathrm{Im}\,\{\langle t_{j_f}|r|u_{opt}(E_n^i)\rangle/(\cos\delta_{opt} + \sin\delta_{opt})\}}{\mathrm{Im}\,(S_{opt})} \right|^2, \quad (5.10b)$$

if $i \neq 0$. The u_{opt} is normalized as in eq. (5.5). The geometrical factor $\mathscr{A}(i)$ depends on the spin of the core in channel i. Its expression can be found in ref. [9]). Of course, if $i = 0$ corresponds to a zero-spin target, $\mathscr{A}(i = 0) = 1/2\pi$ [see eq. (3.6)]. In eq. (5.8), we neglected the local fluctuation of $\Gamma_{\lambda n,i}$ with λ, and we assumed that, in the spirit of the optical model, $\langle \Gamma_{\lambda n,i} \rangle \approx \Gamma_\lambda(E_n^i)$ is a function of the neutron energy in channel i. Cugnon and Mahaux [2]) have investigated the properties of the function $\Gamma_\lambda(E)f(E)$, using a simple model for the energy dependence of $\Gamma_\lambda(E)$. They took for $f(E)$ a formula involving a real potential that reproduces the optical scattering length. At positive energy, they checked that it yields the same results as the expression with a complex potential. Here, we perform the calculation with a complex optical potential on both sides of threshold. The evaluation of $\Gamma_\lambda(E_n)$ is impossible but a closely related quantity is the strength function. Thus, it is better to consider

$$\langle \Gamma_{\lambda f,i} \rangle / D = (\theta_{i,2p})^2 \zeta(i) s(E_n^i) f(E_n^i), \qquad i = 0, 1, 2, \ldots, \quad (5.11)$$

where

$$s(E_n^i) = \langle \Gamma_\lambda(E_n^i) \rangle / D. \quad (5.12)$$

At this point, we have to say a few words about the optical potential in the channels $i \neq 0$. No experimental information is available. Furthermore, the quantities $s(E_n^0)$ and $s(E_n^i)$ cannot be determined independently by an optical-model calculation if there is a strong coupling between channels $i = 0$ and $i \neq 0$, such as the rotational and the vibrational couplings which split the 4s giant resonance in two parts. In the absence of strong coupling, there are not many reasons to believe that the optical-model potential in channels $i \neq 0$ is very different from the optical-model potential in channel $i = 0$, since in general the target state in channel i can be obtained from the ground state by putting a small perturbation near the Fermi surface. Hence, in

the following, we restrict to the 3s and 3p regions and we use the same optical potential for all the channels.

The properties of the strength function $s(E)$ near elastic threshold have been investigated by Goebel and McVoy [13]) and by Lane [8]). An optical-model calculation of the strength function at negative energy has been performed recently [14]). It turns out that the neutron strength function is continuously rising as the energy becomes more and more negative, with a rate which varies, however, from one nucleus to the other.

The results of the calculation of the quantity (5.11) are displayed in fig. 7, where we put $\theta^2 = 1$, and where ζ is given by (5.9) with $\mathscr{A}(i) = 1/2\pi$. They refer to the 3s region and Moldauer's optical potential [9]) is used. The bound state wave function (this is true for fig. 8 also) corresponds to the potential of ref. [11]). The energy of the

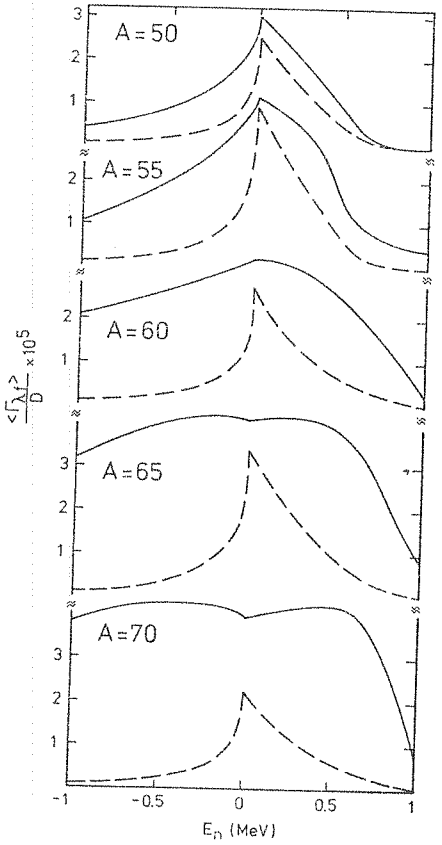

Fig. 7. The 3s region. The dashes represent the function $|k|f$ (see the text), in arbitrary units, and the full curve corresponds to the photon strength function.

transition ε_γ is taken as $\varepsilon_\gamma = E_n^0 + E_B$, where E_B is the binding energy of the 2p state in the potential well of ref. [11]). The dashed curves represent the function $|k|f(E_n)$, with $|k| = \sqrt{2m|E_n|/\hbar^2}$: it shows a cusp at $E_n = 0$ for all the nuclei. This was already noticed in ref. [2]). Moreover, it decreases sufficiently rapidly when E_n becomes more and more negative to compensate in some cases the rise of the function $|k|^{-1}s_n$. This compensation is less and less effective as A increases, and, for $A \gtrapprox 65$, the photon strength function is as big at $E_n < 0$ as at $E_n > 0$. Our calculations confirm the general trend of the results of ref. [2]), although for $A \approx 60$, they indicate that the photon strength function still decreases at negative energy. We also give the absolute value for the photon strength function, while ref. [2]) deals with relative value only.

Our curves can be used for getting an estimate of the contribution due to a given inelastic channel, at least if one knows the level density D^{-1}. However, a safer use of our curves is to deduce from them the ratio between the inelastic to the elastic channel contributions (except for the spectroscopic factor). Of course, one does not know the phase between the two amplitudes, but our calculation gives an idea of the correction to the simple valency model amplitude.

Finally, our curves also give the partial photon strength function below neutron threshold. We see from fig. 7 that this quantity peaks at threshold for $A < 60$, while it is somewhat flat for values of A above 60. This result contrasts with the behaviour of the calculated neutron strength function, which is qualitatively the same for all nuclei [14]).

In fig. 8, we display the results of a similar calculation for the 3p region. Moldauer's optical potential has been used without a spin-orbit term, however, in order to get directly an average of the $p_{\frac{3}{2}}$ and $p_{\frac{1}{2}}$ neutron strength function. The quantity $\zeta(i)$ is

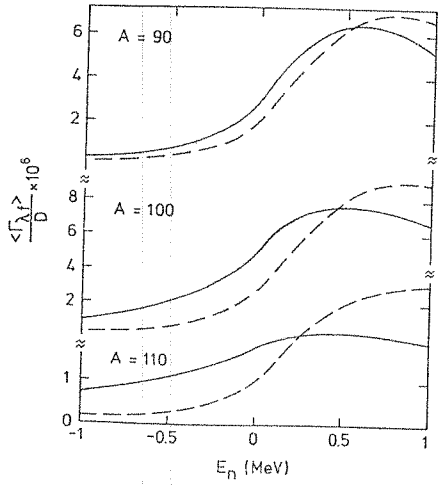

Fig. 8. The 3p region. The dashes represent the function $|k|^3 f$ (see the text) in arbitrary units. The full curves give the photon strength function.

given by (5.9) with $\mathscr{A}(i) = 1/4\pi$. The results indicate that the valency model is expected to work well up to $A \approx 110$. This is very different from the situation in the 3s region, where the model seems to fail in the upper half of the giant resonance region.

6. Conclusions

In this paper, we have investigated several numerical aspects of the valence model for low-energy neutron radiative capture. This model predicts a proportionality factor between neutron and partial photon widths. We have indicated that, apart from a simple kinematical factor, this proportionality factor does not vary very much with the neutron energy. We have calculated this factor for a large part of the periodic table and have presented the graphs in such a way as they are very well suited to the analysis of experimental data. For the 4s region, we have given predictions for the size of the background radiative capture cross section and we have shown the regions where it is more likely to be observed. Finally, we have estimated the inelastic channel contributions in the 3s and 3p regions. Our results indicate that the valence model does not work well in the upper half of the 3s giant resonance, while it works well in almost the whole 3p region. Moreover, in the 3s region, the calculated partial photon strength functions display an interesting threshold effect, whose features change with the mass number.

We thank Dr. A. M. Lane for a useful correspondence and Dr. M. Bawin for a careful reading of the manuscript. We gratefully acknowledge the kind hospitality displayed by the members of the Division de Physique Théorique et Orsay, where part of this work was carried out.

References

1) A. M. Lane, 2nd Int. Symp. on neutron gamma-ray spectroscopy and related topics, RCN, Petten, 1974, p. 31
2) J. Cugnon and C. Mahaux, Ann. of Phys. **94** (1975) 128
3) A. M. Lane and J. E. Lynn, Nucl. Phys. **17** (1960) 563
4) A. M. Lane and J. E. Lynn, Nucl. Phys. **17** (1960) 586
5) A. M. Lane and S. F. Mughabghab, Phys. Rev. **C10** (1974) 412
6) C. Mahaux and H. A. Weidenmüller, Shell-model approach to nuclear reactions (North-Holland, Amsterdam, 1969)
7) H. Feshbach, Ann. of Phys. **5** (1958) 357
8) A. M. Lane, Phys. Lett. **B50** (1974) 207
9) J. E. Lynn, The theory of neutron resonances reactions (Clarendon Press, 1968) p. 328
10) P. A. Moldauer, Nucl. Phys. **47** (1963) 65
11) A. A. Ross, H. Mark and R. D. Lawson, Phys. Rev. **102** (1956) 1613
12) P. A. Jain, Nucl. Phys. **50** (1964) 157
13) C. J. Goebel and K. W. McVoy, Nucl. Phys. **A115** (1968) 504
14) J. Cugnon, Nucl. Phys. **A263** (1976) 47
15) A. J. F. Siegert, Phys. Rev. **52** (1937) 787